catalysts

MDPI

Article

Intrinsic Kinetics Study of Biogas Methanation Coupling with Water Gas Shift over Re-Promoted Ni Bifunctional Catalysts

Xinxin Dong, Baosheng Jin *, Zhiwei Kong and Lu Dong

Key Laboratory of Energy Thermal Conversion and Control of Ministry of Education, School of Energy & Environment, Southeast University, Nanjing 210096, China; xxdong_seu@163.com (X.D.); kong_zhi_wei@163.com (Z.K.); ludong901122@sina.com (L.D.)

* Correspondence: bsjin@seu.edu.cn; Tel.: +86-25-8379-4744

Received: 21 April 2019; Accepted: 2 May 2019; Published: 6 May 2019

Abstract: The intrinsic kinetics of biogas methanation coupling with water gas shift over Re-promoted Ni bifunctional catalysts were investigated in this study. The catalysts were prepared through co-impregnation of Ni and Re precursors on the H_2O_2-modified manganese sand. The experiments were performed in a fixed bed reactor under the assorted reaction conditions of 300–400 °C, 0.1–0.3 MPa, and a 0.6–1.0 H_2/CO ratio. The effect of gas internal and external diffusion on the performance of methanation coupling with water gas shift was examined by changing catalyst particle size and gas hourly space velocity (GHSV) and further verified by the Weisz–Prater and Mears criterion, respectively. It was found that the internal and external diffusions were eliminated when the catalyst particle size was 12–14 meshes and GHSV was 2000 h^{-1}. Three kinetics models including the empirical model (EM), synergetic model (SM), and independent model (IM) were proposed, and 25 sets of experimental data were obtained to solve the model parameters. By mathematical fitting and analysis, it was discovered that the fitting situation of the three kinetics models was in the order of EM > SM > IM, among which EM had the highest fitting degree of 99.7% for CH_4 and 99.9% for CO_2 with the lowest average relative error of 8.9% for CH_4 and 8.7% for CO_2. The over 30% of average relative error for CO_2 in IM might exclude the possibility of the Langmuir–Hinshelwood water gas shift mechanism in the real steps of biogas methanation coupling with water gas shift over Re-promoted Ni catalysts.

Keywords: intrinsic kinetics; biogas; methanation; water gas shift; rhenium; bifunctional catalysts

1. Introduction

The demand for substitutes of traditional fossil energy has been increasingly urgent because of its continuous depletion and the austere environmental problems. Biomass is considered as one of the most promising energy candidates since it is renewable, eco-friendly, as well as massive in production. It is estimated that the potential worldwide biomass energy in 2050 will be between 25×10^9–76×10^9 BOE (barrels of oil energy equivalent) [1]. In the case of China, according to the research conducted by Shi, the total current traditional biomass feedstock is about one billion metric TCE (tons of standard coal equivalent) [2]. The conventional routes to employ biomass are diverse, including combustion to produce heat, pyrolysis to extract bio-oil, and gasification to obtain biogas [3]. Particularly under the background of rapid urbanization in China, converting biomass to biogas by means of gasification is of both social and economic significance, as it not only can supply centralized gas for urban residents, but also could largely reduce the dependence on fossil fuels [4,5].

Due to the issues of high CO content and low heating value, the biogas needs to be upgraded before it is finally transported to downstream users via pipelines. Water gas shift (Equation (1))

is an efficient technical method to reduce the CO content in biogas, and the methanation reaction (Equation (2)) is able to increase the heating value by producing CH_4. As a result, the above two reactions are frequently applied in the upgrading process of biogas into urban gas [6–8]. Traditionally, the two reactions are individually catalyzed by their specified catalyst (water gas shift catalyst and methanation catalyst). If integrating these two reactions into one unit, the upgrading process will be simplified and the cost of equipment will be reduced [9]. In other words, the key factor of the ideal integrated unit for methanation coupling with water gas shift is the bifunctional catalyst, which is capable of catalyzing methanation and water gas shift simultaneously.

$$CO + H_2O \rightarrow CO_2 + H_2 \quad \Delta H^0 = -40.6 kJ/mol \tag{1}$$

$$CO + 3H_2 \rightarrow CH_4 + H_2O \quad \Delta H^0 = -206.1 kJ/mol \tag{2}$$

The research on the dual-functional catalyst for methanation coupling with water gas shift has been continuously reported over the years. Yuan et al. prepared the SiO_2 supported Ni-Ru bimetallic catalyst, which exhibited an outstanding synergistic effect on methanation and water gas shift. The CH_4 and CO_2 selectivity under the condition of 593 K and 1 MPa could reach around 80% and 10%, respectively [10]. Mei combined Co and Ru together to obtain Co-Ru bimetallic nanoparticles for water gas shift. The highest CO conversion of 98.6% exceeding the thermodynamic equilibrium limit could be achieved over $Co/RuO_2/Al_2O_3$ catalyst with Co/Ru = 1, mainly owing to the co-occurrence of methanation [11]. Apart from metallic catalysts, some novel non-metallic catalysts have also been investigated for methanation coupling with water gas shift. For example, Huo et al. [12] applied β-Mo_2C into the process of methanation, and it was demonstrated that the catalyst could catalyze water gas shift at the same time. According to their 100-h stability test, the CH_4 selectivity was maintained at 33.54% accompanied by 38.34% of CO_2 selectivity. In our previous work [13,14], the Re-promoted Ni catalyst was also studied, and it was found that the addition of Re promoter could effectively enhance the synergistic performance for methanation coupling with water gas shift of biogas from both structural and electronic aspects. At the present stage, Ni-based catalyst is in fact the priority choice as an industrial catalyst considering its high activity and relatively low market price [15,16]. The application of Ni-based catalyst is thus comprehensively more competitive in the process of biogas upgrading.

Catalytic science not only concentrates on the formula and activity of one specific catalyst, but also puts extra emphasis on its scale-up production in industry. In this case, intrinsic kinetics study under well-controlled conditions is crucial and inevitable as it provides important information for the understanding of the mechanism of the involved reactions [17] and meanwhile the simulation and choice of reactors [3]. The intrinsic kinetics of single methanation or water gas shift has been intensively studied principally by means of Langmuir–Hinshelwood adsorption equations [18–20] and empirical power-law models [21,22]. For methanation reaction, the mechanism used for intrinsic kinetics study consists of the CO direct dissociative mechanism and the hydrogen associative mechanism [23]; while in the case of water gas shift reaction, both regenerative and associative mechanisms are proposed in the intrinsic kinetics investigation [24]. However, the above-mentioned kinetic models are primarily confined to single reaction (methanation or water gas shift). It is inadequate and inappropriate to study the intrinsic kinetics of methanation coupling with water gas shift if the separate models are employed. Besides, to our best knowledge, relevant research on Ni-Re bifunctional catalyst is scarce. Hence, for the process of biogas upgrading, interpreting the promotion role of Re in the Ni-Re bifunctional catalyst from the perspective of intrinsic kinetics naturally becomes necessary and meaningful.

The present work was undertaken to investigate the intrinsic kinetics of biogas methanation coupling with water gas shift over Ni-Re bifunctional catalysts supported on H_2O_2 modified manganese sand [14], which is abundant in nature and widely applied in the water treatment area. This novel mineral was first employed as catalyst support, and it was promising for industrial application due to its ample resources and easy access. The corresponding experiments were carried out in a self-designed

fixed bed reactor. Three kinetics models including the empirical, synergetic, and independent models for methanation coupling with water gas shift were applied. In order to assess the accuracy of the obtained kinetic parameters, the calculated values were compared with the experimental results under varying operation conditions.

2. Results and Discussion

2.1. Internal/External Diffusion Elimination

The results of internal/external diffusion elimination tests are shown in Figure 1. As can be seen in Figure 1a, the CO conversion, CH_4 selectivity, and CO_2 growth rate all increase when the catalyst particle size decreases from 8–10 meshes to 10–12 meshes, which indicates a languishing effect of internal diffusion on the catalytic performance of methanation coupling with water gas shift. After lowering the catalyst particle size below 12–14 meshes, there is a proximate platform on the changing curves of CO conversion, CH_4 selectivity, and CO_2 growth rate, which stabilizes at around 98.1, 22.3, and 23.4%, respectively. This effectively implies that the effect of internal diffusion is nearly dislodged [25]. The values of the Weisz–Prater criterion in Table S1 also directly prove the above conclusion. As shown in Table S1, both the $N_{W\text{-}P}$ value of methanation reaction and water gas shift decrease with catalyst particle size. Specifically, the $N_{W\text{-}P}$ value of methanation is constantly below 0.3, while water gas shift is larger than 0.3 when the catalyst particle size lies in the range of 8–12 meshes. This indicates that the internal diffusion effect exists under such a particle size, which is in accord with the experimental results in Figure 1a. Besides, it can be deduced that the internal diffusion effect in the range of 8–12 meshes comes mainly from water gas shift. The $N_{W\text{-}P}$ values of both methanation and water gas shift under 12–18 meshes are smaller than 0.3 corresponding to the platform of the changing curves in Figure 1a. Therefore, the particle size of 12–14 meshes was chosen in the subsequent intrinsic kinetics measurements, under which the internal diffusion was considered to be eliminated.

Figure 1b displays the effect of gas hourly space velocity on the performance of methanation coupling with water gas shift. As can be seen, the CO conversion, CH_4 selectivity, and CO_2 growth rate decreased with gas hourly space velocity at the 1000–2000 h^{-1} range and tended to be stable at 2000–3000 h^{-1}. The reducing CO conversion, CH_4 selectivity, and CO_2 growth rate in the range of 1000–2000 h^{-1} were due to depressed contact time between gas-phase reactants and solid-phase catalysts. In this case, the external diffusion effect is significant. While continuing to increase the gas hourly space velocity, the plateau on the changing curves of 2000–3000 h^{-1} demonstrates the marginal gas-solid interfacial resistance, which caused a negligible external diffusion [26,27]. According to the calculation results of the Mears criterion in Table S2, the N_M value of methanation and water gas shift started to be lower than 0.15 from 1500–2500 h^{-1}, respectively. Thus, it appears that the external diffusion should be considered to be eliminated by at least 2500 h^{-1}. However, the Mears criterion belongs to the theoretical reference, which provides a rule to reckon, and the process of obtaining the N_M value is not completely accurate because of some assumed parameters. Hence, on the basis of practical experimental results, gas hourly space velocity of 2000 h^{-1} was chosen in the subsequent intrinsic kinetics measurements, under which the external diffusion was considered to be eliminated.

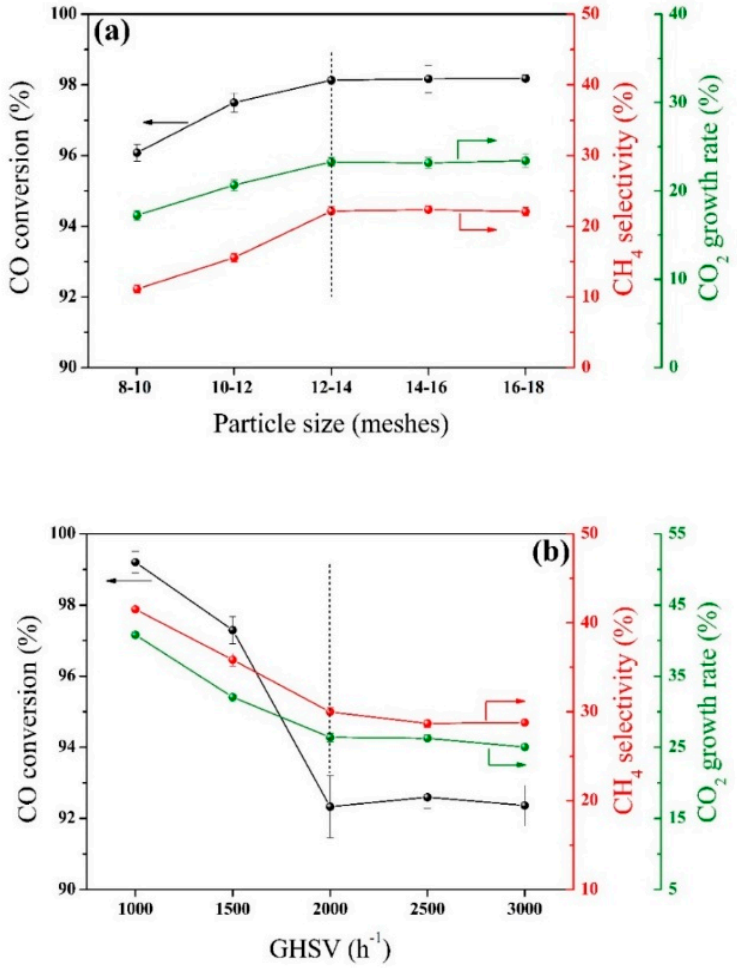

Figure 1. The effect of catalyst particle size (**a**) and gas hourly space velocity (GHSV) (**b**) on the performance of methanation coupling with water gas shift at 350 °C and 0.2 MPa.

2.2. Intrinsic Kinetic Models

The intrinsic kinetics of methanation coupling with water gas shift are expected to be influenced by many factors such as reaction temperature, total pressure and gas composition of both reactants and products. The results of intrinsic kinetics tests based on the orthogonal design in Table S3 using simulated biogas are summarized in Table 1. For the calculative convenience of the following intrinsic kinetic models, the partial pressure of each component and the formation rate of two key products respectively representing methanation and water gas shift, CH_4 and CO_2, were also inventoried.

Table 1. Kinetic data of methanation coupling with water gas shift measured under various reaction conditions.

Case Number	P_{CO} (kPa)	P_{H2} (kPa)	P_{H2O} (kPa)	P_{CO2} (kPa)	P_{N2} (kPa)	r_{CH4} (mol s^{-1} cm^{-3})	r_{CO2} (mol s^{-1} cm^{-3})
1	33.33	20.00	33.33	8.00	5.33	5.84×10^{-7}	2.16×10^{-6}
2	48.03	33.60	48.03	12.24	8.16	9.84×10^{-7}	1.97×10^{-6}
3	61.50	49.30	61.50	16.62	11.08	1.62×10^{-6}	1.46×10^{-6}
4	74.08	66.68	74.08	21.10	14.08	2.01×10^{-6}	9.55×10^{-7}
5	85.71	85.71	85.71	25.71	17.13	2.37×10^{-6}	8.55×10^{-7}
6	32.02	22.40	32.02	8.16	5.44	7.85×10^{-7}	3.95×10^{-6}
7	46.13	36.98	46.13	12.47	8.31	1.09×10^{-6}	2.18×10^{-6}
8	59.26	53.34	59.26	16.88	11.26	1.48×10^{-6}	1.99×10^{-6}
9	71.43	71.43	71.43	21.43	14.28	2.73×10^{-6}	1.25×10^{-6}
10	99.99	60.00	99.99	24.00	15.99	3.61×10^{-6}	8.28×10^{-7}
11	30.75	24.65	30.75	8.31	5.54	9.76×10^{-7}	5.44×10^{-6}
12	44.45	40.01	44.45	12.66	8.45	1.19×10^{-6}	3.16×10^{-6}
13	57.14	57.14	57.14	17.14	11.42	2.04×10^{-6}	2.55×10^{-6}
14	83.33	50.00	83.33	20.00	13.33	3.19×10^{-6}	1.60×10^{-6}
15	96.06	67.20	96.06	24.48	16.32	3.55×10^{-6}	1.02×10^{-6}
16	29.63	26.67	29.63	8.44	5.63	1.08×10^{-6}	6.79×10^{-6}
17	42.86	42.86	42.86	12.86	8.57	1.63×10^{-6}	4.59×10^{-6}
18	66.66	40.00	66.66	16.00	10.66	2.69×10^{-6}	2.05×10^{-6}
19	80.05	56.00	80.05	20.40	13.60	4.27×10^{-6}	2.26×10^{-6}
20	92.25	73.95	92.25	24.93	16.62	5.03×10^{-6}	1.68×10^{-6}
21	28.57	28.57	28.57	8.57	5.71	1.07×10^{-6}	8.53×10^{-6}
22	50.00	30.00	50.00	12.00	8.00	1.89×10^{-6}	4.58×10^{-6}
23	64.04	44.80	64.04	16.32	10.88	3.05×10^{-6}	3.47×10^{-6}
24	76.88	61.63	76.88	20.78	13.85	3.59×10^{-6}	2.48×10^{-6}
25	88.89	80.01	88.89	25.32	16.89	6.45×10^{-6}	2.58×10^{-6}

2.2.1. Empirical Power-Law Model

The empirical power-law model was based on practical experience, which was not derived from any theoretical reaction mechanisms. Even so, the accuracy of this model is not necessarily inferior to those complex and fundamental expressions [22]. Its usefulness as a tool with simplicity has been demonstrated and also recommended in many research works such as the simulation of fuel processing reactors [28] and the determination of reaction kinetics parameters [29,30]. The empirical power-law model for methanation coupling with water gas shift could be defined as the following equations [16,22,31]:

$$r_{CH4} = k_1^0 \exp(-E_1/RT) P_{CO}^{a_1} P_{H2}^{b_1} P_{CH4}^{c_1} P_{H2O}^{d_1} \quad (3)$$

$$r_{CO2} = k_2^0 \exp(-E_2/RT) P_{CO}^{a_2} P_{H2O}^{b_2} P_{H2}^{c_2} P_{CO2}^{d_2} (1-\beta) \quad (4)$$

$$\beta = P_{H2} P_{CO2} / (K_{eq,WGS} P_{CO} P_{H2O}) \quad (5)$$

where r is the formation rate per volume of catalyst (mol s^{-1} cm^{-3}), k^0 is the pre-exponential factor (mol s^{-1} cm^{-3} $kPa^{-(a+b+c+d)}$), E is the activation energy (kJ mol^{-1}), R is the universal gas constant, which equals 8.314 J mol^{-1} K^{-1}, T is the reaction temperature (K), P_i is the partial pressure of component i (kPa), a, b, c, and d are the reaction orders of its corresponding component, β is described as a measure of the reversal water gas shift, and the contained $K_{eq,WGS}$ is the equilibrium constant of water gas shift, which could be calculated from the van't Hoff equation [32,33]. The values of $K_{eq,WGS}$ under different reaction temperatures are summarized in Table S4.

The solution of model parameters requires the basic knowledge of the matrix, and the solving process was assisted by the MATLAB software (described in Section S5). The solved model parameters are listed in Table 2. As can be seen, the reaction rate of methanation presented a positive correlation with CO and H_2 because the increase in the partial pressure of these two reactants will cause their rising concentrations, thus further promoting the reaction. It is interesting to find that H_2O has a positive influence on methanation because the introduction of H_2O will accelerate the water gas shift

reaction whose product is H_2, the essential reactant for methanation. The same phenomenon will also be observed in the water gas shift reaction. Apart from the positive correlation of CO and H_2O, the existence of H_2 in the feed gas will promote water gas shift since it is also involved in the methanation reaction and produces H_2O for water gas shift. From the analysis above, the mutually reinforcing effect can be clearly noted in the reaction process of methanation coupling with water gas shift, and such an effect has also been reported by Lim and his co-workers [34]. Besides, the negative role CO_2 plays in the water gas shift suggests that it should take pretreatment for CO_2 in biogas, which is in accordance with several industrial applications [35–37].

Table 2. Parameters of the empirical model.

Reaction	Reaction Orders *a*	Reaction Orders *b*	Reaction Orders *c*	Reaction Orders *d*	Pre-exponential Factor k^0	Activation Energy *E* (kJ mol^{-1})
Methanation	0.5803	0.2468	0	0.5803	6.290×10^{-7}	23.25
Water gas shift	1.9645	1.9645	4.2979	−9.4584	2.550×10^{-6}	33.48

2.2.2. Synergetic Model

The methanation coupling with water gas shift contains two reactions, and they are influential on each other. To describe its mechanism, it is inadvisable to dissever these two reactions. As a whole, the methanation coupling with water gas shift lacks a thorough understanding in the synergetic effect; thus, their synergetic intrinsic kinetics model remains to be studied. However, Xu and Froment's [38] research on methane steam reforming and water gas shift over Ni catalysts provided some meaningful references for our work. In their work, the coexisting mechanism of methane steam reforming and water gas shift was proposed and the intrinsic kinetics model based on Langmuir–Hinshelwood adsorption equations was concluded. Considering methanation is the reverse reaction of methane steam reforming, the intrinsic kinetics model for methanation coupling with water gas shift does not demand any amendment and is simply modified by changing the plus-minus of the rate equation for methane steam reforming. The involved elementary reactions in the mechanism of methanation coupling with water gas shift are summarized in Table 3, and the derived Xu and Froment intrinsic kinetics model is listed as the following equations, which have been employed and examined by several researchers [39,40].

$$r_{CH4} = \frac{k_1^0 \exp\left(-\frac{E_1}{RT}\right)}{P_{H2}^{2.5}}\left(\frac{P_{CO}P_{H2}^3}{K_{eq,SMR}} - P_{CH4}P_{H2O}\right)/DEN^2 \quad (6)$$

$$r_{CO2} = \frac{k_2^0 \exp\left(-\frac{E_2}{RT}\right)}{P_{H2}}\left(P_{CO}P_{H2O} - \frac{P_{CO2}P_{H2}}{K_{eq,WGS}}\right)/DEN^2 \quad (7)$$

$$DEN = 1 + K_{CO}P_{CO} + K_{H2}P_{H2} + K_{CH4}P_{CH4} + \frac{K_{H2O}P_{H2O}}{P_{H2}} \quad (8)$$

$$K_i = K_i^0 \exp\left(\frac{-\Delta H_i}{RT}\right)\ i = CO, H_2, CH_4,\ H_2O \quad (9)$$

where r (mol s^{-1} cm^{-3}), k^0, E (kJ mol-1), R (8.314 J mol^{-1} K^{-1}), T (K), and P_i (kPa) have the same meanings as in the empirical model of Section 2.2.1, K_i is the adsorption equilibrium constant, K_i^0 is the adsorption pre-exponential factor, and ΔH_i (kJ mol^{-1}) is the enthalpy change of adsorption. The values of $K_{eq,SMR}$ under different reaction temperatures are also listed in Table S4.

Table 3. The elementary reactions involved in the mechanism of methanation coupling with water gas shift.

Number	Elementary Reaction	Instruction
1	$H_2 + 2^* \leftrightharpoons 2H^*$	
2	$CO + ^* \leftrightharpoons CO^*$	
3	$CO^* + ^* \leftrightharpoons C^* + O^*$	
4	$C^* + H^* \leftrightharpoons CH^* + ^*$	
5	$CH^* + H^* \leftrightharpoons CH_2^* + ^*$	RDS
6	$CH_2^* + H^* \leftrightharpoons CH_3^* + ^*$	
7	$CH_3^* + H^* \leftrightharpoons CH_4 + 2^*$	
8	$H_2O + ^* \leftrightharpoons H_2 + O^*$	
9	$CO^* + O^* \leftrightharpoons CO_2^* + ^*$	RDS
10	$CO_2^* \leftrightharpoons CO_2 + ^*$	

*: active site, RDS: rate-determining step.

The parameters of the synergetic model were also obtained through the nonlinear regression algorithm and displayed in Table 4. It should be noted that the E_1 value stands for the activation energy of steam methane reforming reaction rather than methanation reaction, which is comparable to that in the work of Xu and Froment (240.1 kJ mol$^{-1)}$. However, the activation energy E_2 of water gas shift is much lower than the reported value by Xu and Froment (67.13 kJ mol^{-1}), which is a reflection of the promotion effect of Re on the Ni-based catalysts for methanation coupling with water gas shift.

Table 4. Parameters of the synergistic model.

Parameter	Value	Unit
${k_1}^0$	1.216×10^{16}	mol s^{-1} cm^{-3} kPa$^{0.5}$
E_1	221.10	kJ mol^{-1}
${k_2}^0$	18.32	mol s^{-1} cm^{-3} kPa^{-1}
E_2	14.90	kJ mol^{-1}
${K_{CO}}^0$	11.67	kPa^{-1}
ΔH_{CO}	−10.85	kJ mol^{-1}
${K_{H2}}^0$	8.32×10^{-3}	kPa^{-1}
ΔH_{H2}	26.68	kJ mol^{-1}
${K_{H2O}}^0$	7.95×10^{-2}	-
ΔH_{H2O}	17.33	kJ mol^{-1}

2.2.3. Independent Model

The veritable mechanism of methanation coupling with water gas shift over Ni-Re catalyst is still unknown, and the above synergistic model is on the basis of steam methane reforming, which may conclude both methanation and water gas shift reactions. However, it might also be worthwhile to try to employ the separate mechanism of methanation and water gas shift and combine them together to provide a model for intrinsic kinetics investigation. Though such an independent model cannot truly reflect the mechanism of methanation coupling with water gas shift, it is still of significance to use it to approach the fact. In addition, it is also meaningful to apply the independent model to measure the deviation between reality and theory. In this work, the dissociative methanation mechanism of Klose and Baerns [41] and the Langmuir–Hinshelwood water gas shift mechanism proposed by Ayastuy [42] were utilized as independent models to describe the process of methanation coupling with water gas shift, whose involved elementary reactions are listed in Table 5. The final mathematical expressions for these two models are shown in the following:

$$r_{CH4} = k_{CH2} K_C K_H^2 P_{CO}^{0.5} P_{H2} / \left(1 + K_C P_{CO}^{0.5} + K_H P_{H2}^{0.5}\right)^3 \quad (10)$$

$$r_{CO2} = k_{WGS}(P_{CO}P_{H2O} - \frac{P_{CO2}P_{H2}}{K_{eq,WGS}})/(1 + K_{CO}P_{CO} + K_{H2}P_{H2} + K_{CO2}P_{CO2} + K_{H2O}P_{H2O})^2 \quad (11)$$

$$k_i = k_i^0 \exp(\frac{-\Delta E_i}{RT}) i = CH_2, WGS \quad (12)$$

$$K_i = K_i^0 \exp(\frac{-\Delta H_i}{RT}) i = C, H, CO, H_2, CO_2, H_2O \quad (13)$$

where CH_2 and C represent the free radicals that appear during the process of surface adsorption and other parameters have the identical meaning as in the above section. The parameters of these models were solved and are summarized in Table 6.

Table 5. Involved elementary reactions of the independent model.

Number	Dissociative Methanation Mechanism	Langmuir–Hinshelwood Water Gas Shift Mechanism
1	CO + 2* ⇋ C* + O*	CO + * ⇋ CO*
2	H_2 + 2* ⇋ 2H*	H_2O + * ⇋ H_2O*
3	C* + 2H* → H_2C* + 2* or C* + H*⇋*C … H* + H* → H_2C* + 2*	CO* + H_2O* ⇋ CO_2* + H_2*
4	H_2C* + 2H* → CH_4 + 3*	H_2* ⇋ H_2 + *
5	O* + 2H* → H_2O + 3*	CO_2* ⇋ CO_2 + *

*: active site.

Table 6. Parameters of the independent model.

Parameter	Value	Unit
$k_{CH2}{}^0$	12.92	mol s^{-1} cm^{-3}
ΔE_{CH2}	1.42×10^{-2}	kJ mol^{-1}
$k_{WGS}{}^0$	0.35	mol s^{-1} cm^{-3} kPa^{-2}
ΔE_{WGS}	15.18	kJ mol^{-1}
$K_C{}^0$	4.61×10^{-3}	$kPa^{-0.5}$
ΔH_C	15.98	kJ mol^{-1}
$K_H{}^0$	4.41×10^{-3}	$kPa^{-0.5}$
ΔH_H	5.67	kJ mol^{-1}
$K_{CO}{}^0$	35.22	kPa^{-1}
ΔH_{CO}	2.60	kJ mol^{-1}
$K_{H2}{}^0$	2.20×10^{-2}	kPa^{-1}
ΔH_{H2}	95.30	kJ mol^{-1}
$K_{CO2}{}^0$	3.17×10^{-3}	kPa^{-1}
ΔH_{CO2}	83.86	kJ mol^{-1}
$K_{H2O}{}^0$	5.25	kPa^{-1}
ΔH_{H2O}	−12.98	kJ mol^{-1}

2.3. Model Validation and Comparison

In order to examine the qualification of the three selected intrinsic kinetics models, the predicted formation rates of CH_4 and CO_2, which represent two typical products in the methanation coupling with water gas shift, were calculated using the corresponding expressions and further compared to the experimental values. Every model was separately validated, and the results are shown in Figure 2. As can be seen, the predicted rates fit the experimental values to some extent, and the experimental values were basically near the fitted curve. However, there still were some apparent differences between the models. The empirical model appeared to have the best degree of fitting for both methanation and water gas shift reactions, since it considered all the reactants and products in the feeding biogas (CO, H_2, CH_4, H_2O, and CO_2). As suggested by Loc [43], the empirical model can approach the kinetics by not demanding to judge unambiguously the slow step of the reaction, which makes it easier to find the mathematic relationship between reaction rates and reactants. Nevertheless, the limitation of the empirical model is also obvious. It is simply a power-law equation that is not based

on any mechanism, so it cannot reflect any key components in the expression. For the synergetic model, the fitting results were to some extent satisfactory. Though this model was originally proposed by Xu and Froment for analyzing the steam methane reforming coupling with water gas shift over Ni-based catalysts, it still shows adaptability to the methanation coupling with water gas shift in this work. The deviation may come from the difference in reaction conditions. In this work, the reaction temperature and pressure were in the range of 300–400 °C and 0.1–0.3 MPa, which were lower than the employed reaction temperature of 675–1000 K and pressure of 30 bar in Xu and Froment's research. It is considered by many researchers that the reaction conditions have a significant impact on the kinetics models, and every kinetic model is confined to its certain reaction conditions [43–45]. As for the last independent model, the fitting situation for CH_4 and CO_2 is diverse. Judging from the distribution of the experimental values, the formation rate fitting curve for CH_4 was more compact than that for CO_2, implying that the dissociative methanation mechanism might be more suitable than the Langmuir–Hinshelwood water gas shift mechanism to describe the process of methanation coupling with water gas shift. Because the independent model is merely a combination of separate mechanisms, it cannot be assured that this model is appropriate, and from the results of the parity plots, the water gas shift mechanism should be replaced by a more precise model.

To quantitatively measure the deviation degree of experimental values and to compare the three intrinsic kinetic models more directly, the average relative error (ARE) was applied (Equation (14)), and the fitting situations of CH_4 and CO_2 formation rates using three models were integrated in one parity plot (Figure 3). The fitting degree (FD) of the three models was also calculated using Equation (15) and displayed in Figure 4, where r_i^{exp} and r_i^{pre} denote the experimental and predicted formation rate, respectively.

$$\text{ARE}\ (\%) = 100 \times \frac{1}{n} \sum_{i=1}^{n} \left(\left| r_i^{exp} - r_i^{pre} \right| \right) / r_i^{pre} \tag{14}$$

$$\text{FD}\ (\%) = 100 \times \{1 - \left[\frac{\sum_{i=1}^{n} \left(r_i^{exp} - r_i^{pre} \right)^2}{\sum_{i=1}^{n} \left(r_i^{exp} - r_{ave}^{exp} \right)^2} \right] \}, \ r_{ave}^{exp} = \frac{1}{n} \sum_{i=1}^{n} r_i^{exp} \tag{15}$$

As can be seen in Figure 3, the three models presented various discrete situations. Generally, the empirical model possessed the lowest average relative error among three proposed models, which was 8.9% for CH_4 formation rate and 8.7% for CO_2 formation rate. This indicates that the empirical model had a certain general adaptability to diverse reaction conditions. Due to its simple mathematic expressions, the empirical model neglects the actual mechanism of reactions and merely creates a linear relationship between reactants and reaction rates. For the synergetic model and independent model, the fitting situation was the opposite. The average relative error of CH_4 formation rate for the synergetic model was larger than that for the independent model (20.6% vs. 15.3%), while the average relative error of CO_2 formation rate was the reverse (20.9% vs. 34.5%), which implies that both models have flaws. As discussed in the above paragraph, the reaction temperature and pressure in this work were relatively low for the synergetic model. However, from the perspective of statistics, around 20% of average relative error is acceptable, which cannot exclude the possibility of the synergetic mechanism that occurs in the methanation coupling with the water gas shift. The 34.5% of average relative error and 91.8% of fitting degree in Figure 4 for CO_2 formation rate in the independent model suggest that the Langmuir–Hinshelwood water gas shift mechanism may be unsuitable to explain the real steps of water gas shift over Re-promoted Ni catalysts in this work.

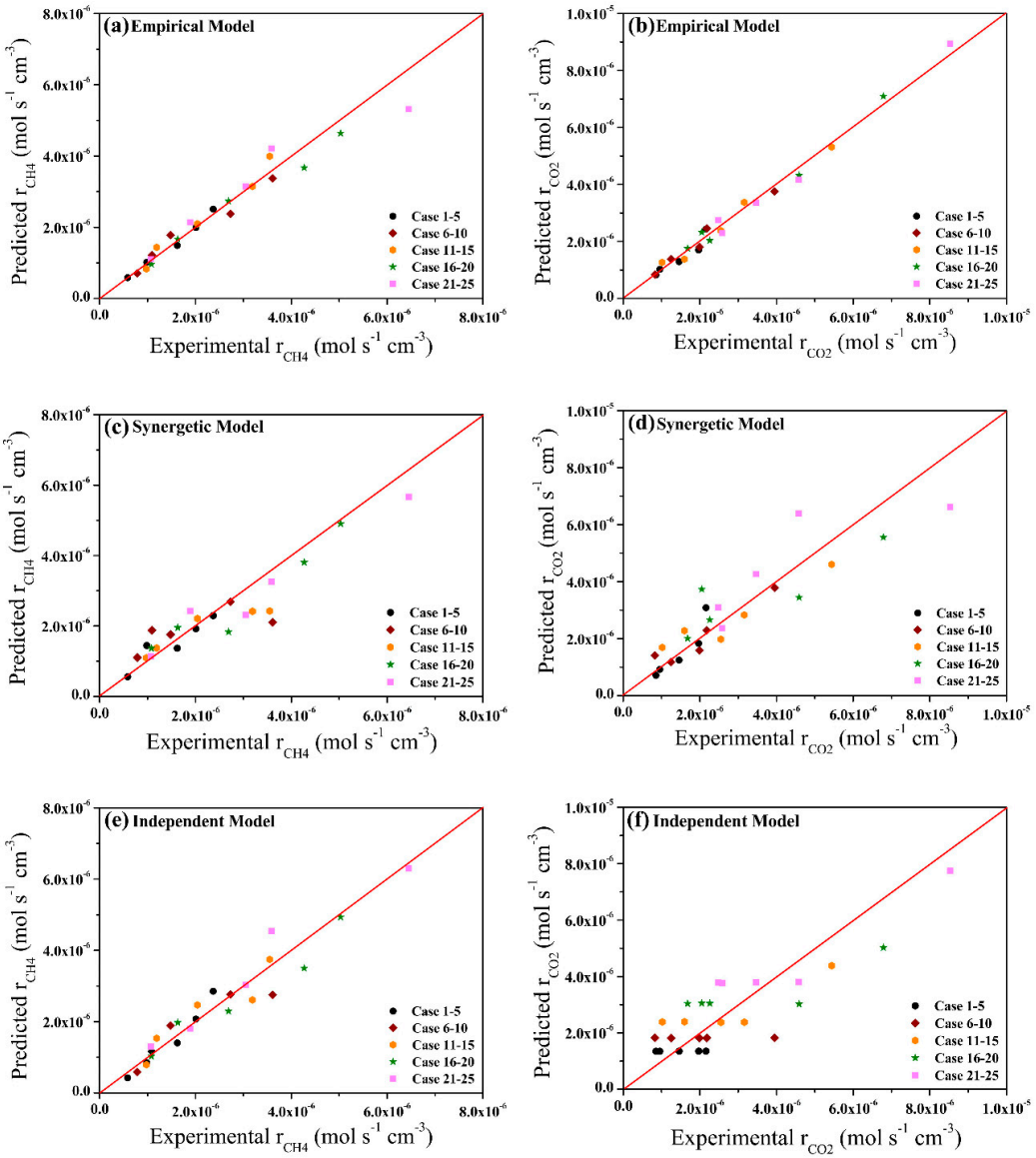

Figure 2. Parity plots of the formation rate of CH_4 and CO_2 for methanation coupling with water gas shift using three kinetic models.

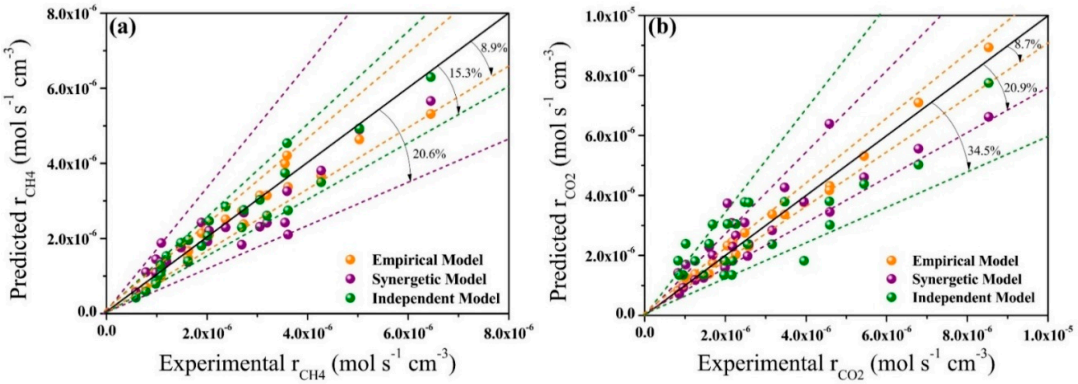

Figure 3. Comparison of three models integrated in one parity plot: (**a**) CH_4 formation rate, (**b**) CO_2 formation rate.

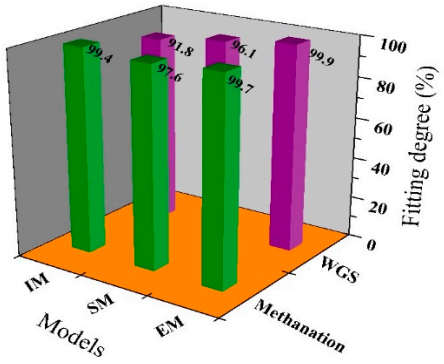

Figure 4. The fitting degree of the three kinetics models for methanation coupling with water gas shift (EM: empirical model, SM: synergetic model, IM: independent model).

3. Materials and Methods

3.1. Catalyst Preparation

The preparation of Ni-Re catalysts supported on H_2O_2 modified manganese sand was divided into two steps. The first step was the modification of the raw manganese sand with H_2O_2 reagent. Specifically, the raw manganese sand was first washed by deionized water and dried in a drying stove. Then, the obtained manganese sand was placed in a 500-mL beaker and mixed with 0.1 mol/L H_2O_2 solution, after which the mixture was kept in a water bath at 80 °C for 4 h and dried overnight. The modified manganese sand (MMS) particle was further ground into 80–100 mesh powder as the final catalyst support, which is denoted as H_2O_2-MMS. The second step was the loading of Ni and Re on the H_2O_2-MMS support by the co-impregnation method. In detail, a precalculated amount of $Ni(NO_3)_2$ and NH_4ReO_4 solution was first mixed with H_2O_2-MMS support and maintained in a water bath at 60 °C for 10 h. After drying, the catalyst precursor was transferred into a muffle furnace and calcined at 400 °C for 5 h. The obtained sample was ground into powder and subsequently compressed into tablets for further use. By this time, the as-prepared catalyst was marked as Ni-Re/H_2O_2-MMS with the 15 wt % Ni and 1 wt % Re designed content.

3.2. Reactor System

A schematic diagram of the three-unit experimental apparatus including gas feeding, gas reaction, and gas analysis is shown in Figure 5. The mass flow rate of inlet gas with the required composition was controlled and measured by a set of mass flowmeters (Sevenstar Co., Ltd., Beijing, China). All the reactant gases were of 99.99% purity (Shangyuan Co., Ltd., Nanjing, China). A peristaltic pump was applied to generate a steady flow of deionized water while an evaporator was used to vaporize the water for steam production. In order to avoid steam condensation, the stainless steel tube connecting the evaporator and the reactor was wrapped with a heating belt, which was heated at around 200 °C. The fixed bed reactor constructed from stainless steel tube possessed an inner diameter of 50 mm and a length of 1000 mm. The catalyst sample was packed in the middle of the reactor tube sustained by a stainless steel shim. For temperature controlling, a K-type thermocouple was inserted inside the catalyst bed while a pressure gage welded in the top flange and a backpressure valve in the outlet pipe were employed to observe and control the inner reaction pressure, respectively. The outlet gas after reaction was first dehydrated in a cold trap and further deeply removed of moisture by silica gel. For the convenience of gas analysis, the outlet gas was collected in an air bag. The composition of outlet gas was then analyzed by a gas chromatography (Shimadzu GC2018, Kyoto, Japan), which was equipped with a packed column and a molecular sieve column using He as the carrier gas. The separated gas component was accurately detected by a TCD and FID detector, and its corresponding signal was recorded in a workstation for further calculation.

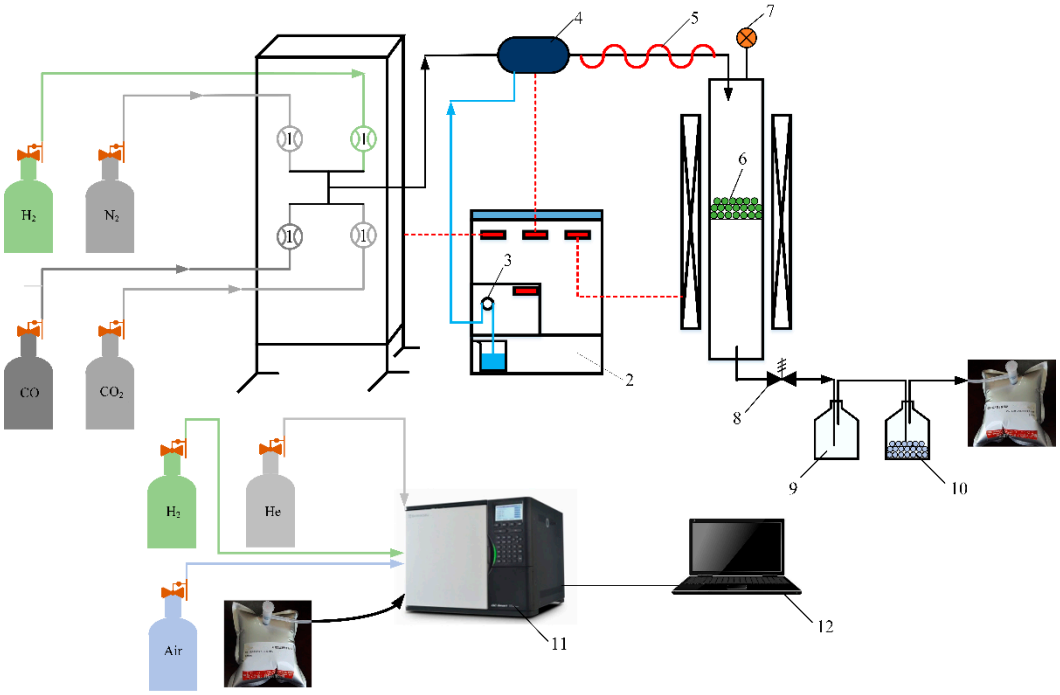

1. Mass Flow Meter 2. Control Panel 3. Peristaltic Pump 4. Steam Generator 5. Heating Belt 6. Catalysts 7. Pressure Gage 8. Backpressure Valve 9. Cold Trap 10. Allochroic Silica Gel 11. Gas Chromatography 12. Workstation

Figure 5. Schematic diagram of the fixed bed reactor system.

3.3. Intrinsic Kinetics Measurements

3.3.1. Inlet Biogas Composition and Operating Conditions

The inlet biogas investigated in this study was specifically composed of a low H_2/CO ratio (H_2/CO ≤1), which might be encountered in the actual biomass gasification process using various feedstock (e.g., microalgae, wood sawdust, wheat straw, and rice straw) and gasifying agents (e.g., water, CO_2, and oxygen-enriched air) [46–49]. In this case, the dry base of inlet biogas composition included an alterable 0.6–1.0 H_2/CO ratio, as well as fixed 12% CO_2 and 8% N_2. The additional steam mixed with the dry inlet biogas was strictly controlled to give a constant H_2O/CO molar flow ratio of 1:1. Table 7 summarizes the entire inlet biogas compositions. In terms of operating conditions, reaction temperature and pressure were chosen as two influential parameters, which ranged from 300–400 °C and 0.1–0.3 MPa, with an interval of 25 °C and 0.05 MPa, respectively.

Table 7. Inlet biogas compositions (dry base) and required steam used in the intrinsic kinetics study.

H_2/CO Ratio	Dry Base Compositions				H_2O/CO Molar Flow Ratio
	H_2 (%)	CO (%)	CO_2 (%)	N_2 (%)	
0.6	30.0	50.0	12.0	8.0	1.0
0.7	32.9	47.1	12.0	8.0	1.0
0.8	35.6	44.4	12.0	8.0	1.0
0.9	37.9	42.1	12.0	8.0	1.0
1.0	40.0	40.0	12.0	8.0	1.0

3.3.2. Internal/External Diffusion Elimination and Verification

The elimination of internal diffusion was practiced by changing the particle size of the catalysts and meanwhile maintaining the catalyst bed volume and gas hourly space velocity. A reaction condition of 350 °C, 0.2 MPa, and 2000 h^{-1} was employed, and the H_2/CO ratio of feed biogas was chosen to be 0.8.

As for the catalyst packing quantity, 30 mL of catalysts were utilized to evaluate the catalyst activity. The overall catalyst activity of methanation coupling with water gas shift could be reflected by the conversion of CO (X_{CO}), the selectivity of CH_4 (S_{CH4}), and the growth rate of CO_2 (R_{CO2}) expressed by Equations (16)–(18), where F stands for the molar flow of the inlet and outlet species (mol s^{-1}). Five parallel comparative tests using catalysts with different particle sizes (8–10, 10–12, 12–14, 14–16, and 16–18 meshes, shown in Figure S2) were conducted to select the suitable catalyst particle size, under which the internal diffusion could be neglected. The elimination of internal diffusion was verified by the Weisz–Prater criterion (Equation (19)) [50], where r denotes the reaction rate per volume of catalyst (mol s^{-1} cm^{-3}), R is the catalyst particle radius (cm), C_s is the reactant concentration at the particle surface (mol cm^{-3}), and D_{eff} is the effective diffusivity (cm^2 s^{-1}).

The elimination of external diffusion was practiced by changing the gas hourly space velocity while keeping the catalyst volume and their particle size as constant in the meantime. When performing the experiments, 30 mL of catalysts with 12–14 meshes were employed, and a reaction condition of 350 °C and 0.2 MPa was inflicted. Like the above experimental design of internal diffusion elimination, the H_2/CO ratio of feed biogas was also set as 0.8. Another five parallel comparative tests under different gas hourly space velocities (1000, 1500, 2000, 2500, and 3000 h^{-1}) were carried out to choose a proper gas hourly space velocity, under which the external diffusion was negligible. The elimination of external diffusion was verified by the Mears criterion (Equation (20)) [51,52], where r refers to the reaction rate per volume of catalyst (mol s^{-1} cm^{-3}), R is the catalyst particle radius (cm), n is the reaction order, k_c is the mass transfer coefficient (cm s^{-1}), and C_b is the concentration of reactant in the bulk phase (mol cm^{-3}).

$$X_{CO}(\%) = ([F_{CO}]_{in} - [F_{CO}]_{out})/[F_{CO}]_{in} \times 100 \quad (16)$$

$$S_{CH4}(\%) = [F_{CH4}]_{out}/([F_{CO}]_{in} + [F_{CO2}]_{in} - [F_{CO}]_{out} - [F_{CO2}]_{out}) \times 100 \quad (17)$$

$$R_{CO2}(\%) = ([F_{CO2}]_{out} - [F_{CO2}]_{in})/[F_{CO2}]_{in} \times 100 \quad (18)$$

$$N_{W-P} = rR^2/(C_s D_{eff}) \leq 0.3 \quad (19)$$

$$N_M = rRn/(k_c C_b) < 0.15 \quad (20)$$

3.3.3. Intrinsic Kinetics Test Procedure

According to the results from the experiments of internal/external diffusion elimination, the catalyst particle size and gas hourly space velocity were determined to be 12–14 meshes and 2000 h^{-1}, respectively. The reasons for choosing the above particle size and gas hourly space velocity are discussed in the Results and Discussion Section 2.1. To examine whether the stainless tube would have a catalytic effect on the feeding gas, a blank test was carried out, and no significant change in the gas composition was observed within the range of selected reaction conditions in this study. Afterwards, 30 mL of catalysts were carefully placed in the reactor tube as the catalyst bed. For a typical intrinsic kinetics measurement, the catalysts were initially reduced under 450 °C for 4 h using a pure H_2 stream with a gas hourly space velocity of 1000 h^{-1}. After the reduction was completed, the catalyst bed was cooled to the desired temperature under a N_2 stream and then switched to the reaction gas mixture with a certain composition. All the reaction cases were designed by the orthogonal experimental method and are listed in Table S3.

4. Conclusions

The intrinsic kinetics of biogas methanation coupling with water gas shift over Re-promoted Ni catalysts were first investigated under a wide range of reaction conditions, including various biogas H_2/CO ratios, temperatures, and pressures. Before the intrinsic kinetics tests, a couple of experiments were designed to examine the influence of internal and external diffusion on the catalyst performance by changing the catalyst particle size and gas hourly space velocity, respectively. According to the Weisz–Prater criterion, the internal diffusion was considered to be eliminated when the catalyst particle

size was 12–14 meshes. In addition, the external diffusion was negligible when the gas hourly space velocity was 2000 h^{-1} based on the Mears criterion. Three kinetics models including the empirical model, synergetic model, and independent model were proposed to clarify the intrinsic kinetics of methanation coupling with water gas shift. Twenty five cases in total were employed to obtain the corresponding parameters for the three models, among which the empirical model had the highest 99.7% fitting degree for CH_4 formation rate and 99.9% fitting degree for CO_2 formation rate. The around 20% of average relative error for the synergetic model is acceptable to some extent, which implies the possibility of a synergetic mechanism occurring in the methanation coupling with water gas shift. However, it seems that the Langmuir–Hinshelwood water gas shift mechanism might be unsuitable because of its relatively larger average relative error between the predicted and experimental values.

Supplementary Materials: The following are available online at http://www.mdpi.com/2073-4344/9/5/422/s1: Figure S1: MATLAB solving results of the empirical model; Figure S2: Pictures of the prepared catalysts with different particle sizes; Table S1: The parameters of the Weisz–Prater criterion at various catalyst particle sizes; Table S2: The parameters of the Mears criterion at various gas hourly space velocities; Table S3: Orthogonal array; Table S4: Equilibrium constant of methanation and water gas shift under different reaction temperatures.

Author Contributions: Conceptualization, X.D. and B.J.; methodology, X.D.; validation, B.J.; formal analysis, X.D.; investigation, X.X., Z.K., and L.D.; resources, X.D.; data curation, X.D.; writing, original draft preparation, X.D.; writing, review and editing, X.D. and B.J.; funding acquisition, B.J.

Funding: This research was funded by the National Key R&D Program of China (2018YFC1901200), the International S&T Cooperation Program of China (ISTCP, 2014DFE70150), the Scientific Research Foundation of the Graduate School of Southeast University (YBJJ1803), and the U.K.-China Joint Research and Innovation Partnership Fund provided by China Scholarship Council and The British Council (201703780063).

Acknowledgments: The authors would like to sincerely acknowledge Duo Fang at the School of Engineering, The University of Edinburgh, for his assistance in mathematic programming.

Conflicts of Interest: The authors declare no conflict of interest. The funders had no role in the design of the study; in the collection, analyses, or interpretation of data; in the writing of the manuscript; nor in the decision to publish the results.

Nomenclature

F	molar flow of species, mol s^{-1}	K_{eq}	reaction equilibrium constant
r	reaction rate per volume of catalyst, mol s^{-1} cm^{-3}	K_i	adsorption equilibrium constant of component i
R	catalyst particle radius, cm	K_i^0	adsorption pre-exponential factor
C_s	reactant concentration at the particle surface, mol cm^{-3}	ΔH	enthalpy change of adsorption, kJ mol^{-1}
C_b	reactant concentration in the bulk phase, mol cm^{-3}		Greek symbols
D_{eff}	effective diffusivity, cm^2 s^{-1}	ε	catalyst porosity
D_{AB}	binary gas phase diffusion coefficient, cm^2 s^{-1}	τ	tortuosity factor
T	reaction temperature, K	ν	kinetic viscosity, cm^2 s^{-1}
M	molecular weight		Subscript
P	total reaction pressure, bar	in	inlet
n	reaction order	out	outlet
k_c	mass transfer coefficient, cm s^{-1}	ave	average
L	characteristic length, cm		Superscript
u	fluid velocity, cm s^{-1}	exp	experimental
k^0	pre-exponential factor	pre	predicted
E	activation energy, kJ mol^{-1}		
P_i	partial pressure of component i, kPa		

References

1. Huber, G.W.; Iborra, S.; Corma, A. Synthesis of transportation fuels from biomass: chemistry, catalysts, and engineering. *Chem. Rev.* **2006**, *106*, 4044–4098. [CrossRef] [PubMed]

2. Qin, Z.; Zhuang, Q.; Cai, X.; He, Y.; Huang, Y.; Jiang, D.; Lin, E.; Liu, Y.; Tang, Y.; Wang, M.Q. Biomass and biofuels in China: toward bioenergy resource potentials and their impacts on the environment. *Renew. Sustain. Energy Rev.* **2018**, *82*, 2387–2400. [CrossRef]
3. Zhang, J.; Fatah, N.; Capela, S.; Kara, Y.; Guerrini, O.; Khodakov, A.Y. Kinetic investigation of carbon monoxide hydrogenation under realistic conditions of methanation of biomass derived syngas. *Fuel* **2013**, *111*, 845–854. [CrossRef]
4. Yu, L.; Song, M.; Wei, Y.; Xiao, J. Combining carbon fibers with Ni/γ–Al_2O_3 used for syngas production: part A: preparation and evaluation of complex carrier catalysts. *Catalysts* **2018**, *8*, 658. [CrossRef]
5. Wei, Y.; Song, M.; Yu, L.; Gao, R.; Meng, F.; Xiao, J.; Zhang, Y. Promotion effect of SiO_2 on the catalytic performance of Ni/CF for biomass derived gas reforming. *Ind. Eng. Chem. Res.* **2018**, *57*, 10851–10858. [CrossRef]
6. Khan, I.U.; Othman, M.H.D.; Hashim, H.; Matsuura, T.; Ismail, A.F.; Rezaei-DashtArzhandi, M.; Azelee, I.W. Biogas as a renewable energy fuel-a review of biogas upgrading, utilisation and storage. *Energy Convers. Manage.* **2017**, *150*, 277–294. [CrossRef]
7. Angelidaki, I.; Treu, L.; Tsapekos, P.; Luo, G.; Campanaro, S.; Wenzel, H.; Kougias, P.G. Biogas upgrading and utilization: current status and perspectives. *Biotechnol. Adv.* **2018**, *36*, 452–466. [CrossRef] [PubMed]
8. Walker, S.B.; Sun, D.; Kidon, D.; Siddiqui, A.; Kuner, A.; Fowler, M.; Simakov, D.S.A. Upgrading biogas produced at dairy farms into renewable natural gas by methanation. *Int. J. Energy Res.* **2018**, *42*, 1714–1728. [CrossRef]
9. Dong, X.; Song, M.; Jin, B.; Zhou, Z.; Yang, X. The synergy effect of Ni-M (M=Mo, Fe, Co, Mn or Cr) bicomponent catalysts on partial methanation coupling with water gas shift under low H_2/CO conditions. *Catalysts* **2017**, *7*, 51. [CrossRef]
10. Yuan, C.; Yao, N.; Wang, X.; Wang, J.; Lv, D.; Li, X. The SiO_2 supported bimetallic Ni-Ru particles: a good sulfur-tolerant catalyst for methanation reaction. *Chem. Eng. J.* **2015**, *260*, 1–10. [CrossRef]
11. Mei, Z.; Li, Y.; Fan, M.; Argyle, M.D.; Tang, J. The effects of bimetallic Co-Ru nanoparticles on Co/RuO_2/Al_2O_3 catalysts for the water gas shift and methanation. *Int. J. Hydrogen Energy* **2014**, *39*, 14808–14816. [CrossRef]
12. Huo, X.; Wang, Z.; Huang, J.; Zhang, R.; Fang, Y. Bulk Mo and Co-Mo carbides as catalysts for methanation. *Catal. Commun.* **2016**, *79*, 39–44. [CrossRef]
13. Dong, X.; Jin, B.; Sun, Y.; Shi, K.; Yu, L. Re-promoted Ni-Mn bifunctional catalysts prepared by microwave heating for partial methanation coupling with water gas shift under low H_2/CO conditions. *Appl. Catal. A* **2018**, *552*, 105–116. [CrossRef]
14. Dong, X.; Jin, B.; Sun, Y.; Yu, L. Urban gas production from low H_2/CO biogas using Re-promoted Ni catalysts supported on modified manganese sand. *Fuel* **2018**, *220*, 60–71. [CrossRef]
15. Ding, M.; Tu, J.; Zhang, Q.; Wang, M.; Tsubaki, N.; Wang, T.; Ma, L. Enhancement of methanation of bio-syngas over CeO_2-modified Ni/Al_2O_3 catalysts. *Biomass Bioenergy* **2016**, *85*, 12–17. [CrossRef]
16. Li, Z.; Zhang, K.; Wang, W.; Qu, J.; Tian, Y.; Wang, B.; Ma, X. Kinetics of sulfur-resistant methanation over supported molybdenum-based catalyst. *J. Taiwan Inst. Chem. E.* **2016**, *68*, 239–245. [CrossRef]
17. Hla, S.S.; Park, D.; Duffy, G.J.; Edwards, J.H.; Roberts, D.G.; Ilyushechkin, A.; Morpeth, L.D.; Nguyen, T. Kinetics of high-temperature water-gas shift reaction over two iron-based commercial catalysts using simulated coal-derived syngases. *Chem. Eng. J.* **2009**, *146*, 148–154. [CrossRef]
18. Lefebvre, J.; Bajohr, S.; Kolb, T. A comparison of two-phase and three phase CO_2 methanation reaction kinetics. *Fuel* **2019**, *239*, 896–904. [CrossRef]
19. Lim, J.Y.; McGregor, J.; Sederman, A.J.; Dennis, J.S. Kinetic studies of the methanation of CO over a Ni/γ-Al_2O_3 catalyst using a batch reactor. *Chem. Eng. Sci.* **2016**, *146*, 316–336. [CrossRef]
20. Queiroz, G.A.; Menezes Barbosa, C.M.B.; Abreu, C.A.M. Mechanism-based kinetics of the water-gas shift reaction at low temperature with a ruthenium catalysts. *React. Kinet. Mech. Catal.* **2018**, *123*, 573–583. [CrossRef]
21. Roensch, S.; Koechermann, J.; Schneider, J.; Matthischke, S. Global reaction kinetics of CO and CO_2 methanation for dynamic process modeling. *Chem. Eng. Technol.* **2016**, *39*, 208–218. [CrossRef]
22. Hla, S.S.; Sun, Y.; Duffy, G.J.; Morpeth, L.D.; Ilyushechkin, A.; Cousins, A.; Roberts, D.G.; Edwards, J.H. Kinetics of the water-gas shift reaction over a $La_{0.7}Ce_{0.2}FeO_3$ perovskite-like catalyst using simulated coal-derived syngas at high temperature. *Int. J. Hydrogen Energy* **2011**, *36*, 518–527. [CrossRef]

23. Miao, B.; Ma, S.S.K.; Wang, X.; Su, H.; Chan, S.H. Catalysis mechanisms of CO_2 and CO methanation. *Catal. Sci. Technol.* **2016**, *6*, 4048–4058. [CrossRef]
24. Smith, B.R.J.; Loganathan, M.; Shantha, M.S. A review of the water gas shift reaction kinetics. *Int. J. Chem. Reactor Eng.* **2010**, *8*. [CrossRef]
25. Guichard, B.; Gaulier, F.; Barbier, J.; Corre, T.; Bonneau, J.; Levitz, P.; Espinat, D. Asphaltenes diffusion/adsorption through catalyst alumina supports-influence on catalytic activity. *Catal. Today* **2018**, *305*, 49–57. [CrossRef]
26. Vernuccio, S.; Dempfle, D.; Goy, R.; Medlock, J.; Rudolf Von Rohr, P. External mass transfer in a laser sintered structured reactor for continuous hydrogenation of alkynes. *Chem. Eng. Process.* **2018**, *126*, 74–80. [CrossRef]
27. Grilc, M.; Likozar, B. Levulinic acid hydrodeoxygenation, decarboxylation and oligmerization over $NiMo/Al_2O_3$ catalyst to bio-based value-added chemicals: modelling of mass transfer, thermodynamics and micro-kinetics. *Chem. Eng. J.* **2017**, *330*, 383–397. [CrossRef]
28. Choi, Y.; Stenger, H.G. Water gas shift reaction kinetics and reactor modeling for fuel cell grade hydrogen. *J. Power Sources* **2003**, *123*, 432–439. [CrossRef]
29. Koryabkina, N.A.; Phatak, A.A.; Ruettinger, W.F.; Farrauto, R.J.; Ribeiro, F.H. Determination of kinetic parameters for the water-gas shift reaction on copper catalysts under realistic conditions for fuel cell applications. *J. Catal.* **2003**, *217*, 233–239. [CrossRef]
30. Lei, Y.; Cant, N.W.; Trimm, D.L. Kinetics of the water-gas shift reaction over a rhodium-promoted iron–chromium oxide catalyst. *Chem. Eng. J.* **2005**, *114*, 81–85. [CrossRef]
31. Hla, S.S.; Duffy, G.J.; Morpeth, L.D.; Cousins, A.; Roberts, D.G.; Edwards, J.H. Investigation of the effect of total pressure on performance of the catalytic water-gas shift reaction using simulated coal-derived syngases. *Catal. Commun.* **2009**, *11*, 272–275. [CrossRef]
32. Chein, R.; Yu, C.; Wang, C. Numerical simulation on the effect of operating conditions and syngas compositions for synthetic natural gas production via methanation reaction. *Fuel* **2016**, *185*, 394–409. [CrossRef]
33. Molino, A.; Braccio, G. Synthetic natural gas SNG production from biomass gasification-thermodynamics and processing aspects. *Fuel* **2015**, *139*, 425–429. [CrossRef]
34. Lim, J.Y.; McGregor, J.; Sederman, A.J.; Dennis, J.S. The role of the Boudouard and water–gas shift reactions in the methanation of CO or CO_2 over $Ni/\gamma\text{-}Al_2O_3$ catalyst. *Chem. Eng. Sci.* **2016**, *152*, 754–766. [CrossRef]
35. He, Q.; Yu, G.; Yan, S.; Dumée, L.F.; Zhang, Y.; Strezov, V.; Zhao, S. Renewable CO_2 absorbent for carbon capture and biogas upgrading by membrane contactor. *Sep. Purif. Technol.* **2018**, *194*, 207–215. [CrossRef]
36. Baccioli, A.; Antonelli, M.; Frigo, S.; Desideri, U.; Pasini, G. Small scale bio-LNG plant: comparison of different biogas upgrading techniques. *Appl. Energy* **2018**, *217*, 328–335. [CrossRef]
37. Zhang, Y.; Ji, X.; Xie, Y.; Lu, X. Thermodynamic analysis of CO_2 separation from biogas with conventional ionic liquids. *Appl. Energy* **2018**, *217*, 75–87. [CrossRef]
38. Xu, J.G.; Froment, G.F. Methane steam reforming, methanation and water-gas shift: I. intrinsic kinetics. *AIChE J.* **1989**, *35*, 88–96.
39. Materazzi, M.; Grimaldi, F.; Foscolo, P.U.; Cozens, P.; Taylor, R.; Chapman, C. Analysis of syngas methanation for bio-SNG production from wastes: kinetic model development and pilot scale validation. *Fuel Process. Technol.* **2017**, *167*, 292–305. [CrossRef]
40. Parlikkad, N.R.; Chambrey, S.; Fongarland, P.; Fatah, N.; Khodakov, A.; Capela, S.; Guerrini, O. Modeling of fixed bed methanation reactor for syngas production: operating window and performance characteristics. *Fuel* **2013**, *107*, 254–260. [CrossRef]
41. Klose, J.; Baerns, M. Kinetics of the methanation of carbon monoxide on an alumina-supported nickel catalyst. *J. Catal.* **1984**, *85*, 105–116. [CrossRef]
42. Mendes, D.; Chibante, V.; Mendes, A.; Madeira, L.M. Determination of the low-temperature water-gas shift reaction kinetics using a Cu-based catalyst. *Ind. Eng. Chem. Res.* **2010**, *49*, 11269–11279. [CrossRef]
43. Engelbrecht, N.; Chiuta, S.; Everson, R.C.; Neomagus, H.W.J.P.; Bessarabov, D.G. Experimentation and CFD modelling of a microchannel reactor for carbon dioxide methanation. *Chem. Eng. J.* **2017**, *313*, 847–857. [CrossRef]
44. Gayubo, A.G.; Valle, B.; Aramburu, B.; Montero, C.; Bilbao, J. Kinetic model considering catalyst deactivation for the steam reforming of bio-oil over $Ni/La_2O_3\text{-}\alpha Al_2O_3$. *Chem. Eng. J.* **2018**, *332*, 192–204. [CrossRef]

45. Falbo, L.; Martinelli, M.; Visconti, C.G.; Lietti, L.; Bassano, C.; Deiana, P. Kinetics of CO_2 methanation on a Ru-based catalyst at process conditions relevant for Power-to-Gas applications. *Appl. Catal. B* **2018**, *225*, 354–363. [CrossRef]
46. Link, S.; Tran, K.; Bach, Q.; Yrjas, P.; Lindberg, D.; Arvelakis, S.; Rosin, A. Catalytic effect of oil shale ash on CO_2 gasification of leached wheat straw and reed chars. *Energy* **2018**, *152*, 906–913. [CrossRef]
47. Jin, F.; Sun, H.; Wu, C.; Ling, H.; Jiang, Y.; Williams, P.T.; Huang, J. Effect of calcium addition on Mg-AlO_x supported Ni catalysts for hydrogen production from pyrolysis-gasification of biomass. *Catal. Today* **2018**, *309*, 2–10. [CrossRef]
48. Liu, L.; Huang, Y.; Cao, J.; Liu, C.; Dong, L.; Xu, L.; Zha, J. Experimental study of biomass gasification with oxygen-enriched air in fluidized bed gasifier. *Sci. Total Environ.* **2018**, *626*, 423–433. [CrossRef]
49. Duan, P.; Li, S.; Jiao, J.; Wang, F.; Xu, Y. Supercritical water gasification of microalgae over a two-component catalyst mixture. *Sci. Total Environ.* **2018**, *630*, 243–253. [CrossRef]
50. Bui, P.P.; Oyama, S.T.; Takagaki, A.; Carrow, B.P.; Nozaki, K. Reactions of 2-methyltetrahydropyran on silica-supported nickel phosphide in comparison with 2-methyltetrahydrofuran. *ACS Catal.* **2016**, *6*, 4549–4558. [CrossRef]
51. Mohagheghi, M.; Bakeri, G.; Saeedizad, M. Study of the effects of external and internal diffusion on the propane dehydrogenation reaction over Pt-Sn/Al_2O_3 catalyst. *Chem. Eng. Technol.* **2007**, *30*, 1721–1725. [CrossRef]
52. Lee, W.; Wang, Z.; Zheng, W.; Vlachos, D.G.; Bhan, A. Vapor phase hydrodeoxygenation of furfural to 2–methylfuran on molybdenum carbide catalysts. *Catal. Sci. Technol.* **2014**, *4*, 2340. [CrossRef]

© 2019 by the authors. Licensee MDPI, Basel, Switzerland. This article is an open access article distributed under the terms and conditions of the Creative Commons Attribution (CC BY) license (http://creativecommons.org/licenses/by/4.0/).